Supplementary Information

Experimental and Theoretical investigation on change storage performance of $NiSb_2O_6$ and its reduced graphene oxide composite – A Comparative analysis

Parul[1], Surjit Sahoo[2], Satyajit Ratha[1], Gopal Sanyal[3], Brahmananda Chakraborty[4,5]* Saroj Kumar Nayak[1]*

[1]Indian Institute of Technology Bhubaneswar, Argul, Jatani, Khordha, Odisha-752050, India

[2]Department of Mechanical Engineering, Indian Institute of Technology Jammu, Jammu 181221, India

[3]Technology Transfer and Collaboration Division, Bhabha Atomic Research Centre, Trombay, Mumbai-400085, India

[4]High Pressure & Synchroton Radiation Physics Division, Bhabha Atomic Research Centre, Trombay, Mumbai-400085, India

[5]Homi Bhabha National Institute, Mumbai-400094, India

*Email address: nayaks@iitbbs.ac.in, brahma@barc.gov.in

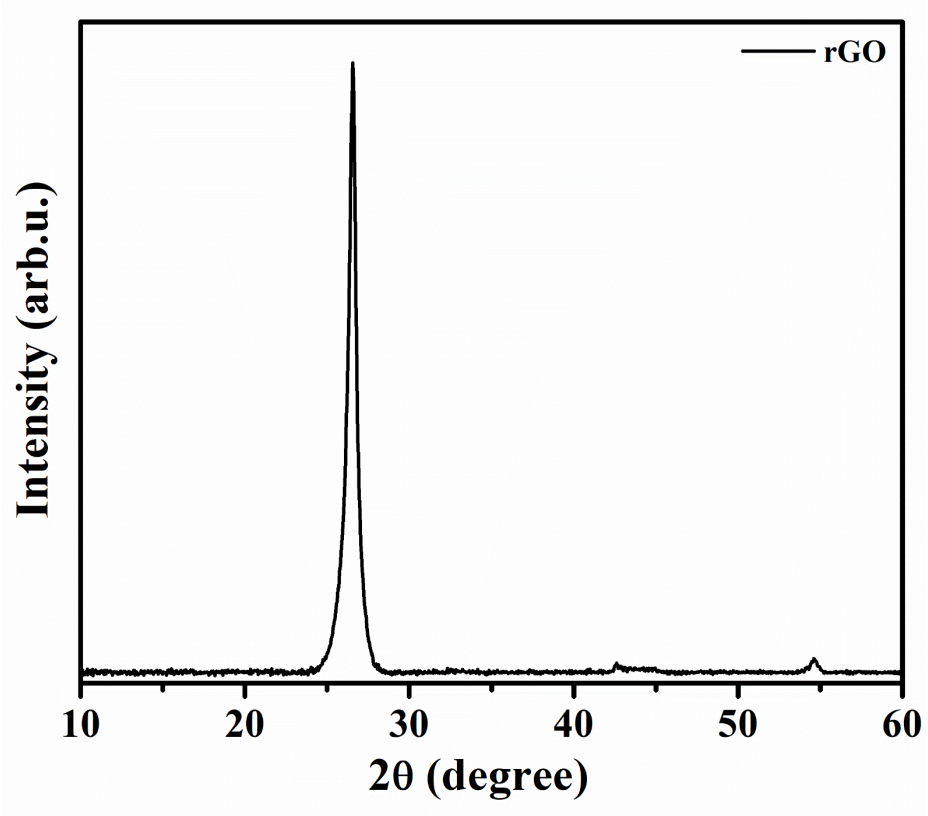

Figure S1 XRD pattern for reduced graphene oxide sample, showing a Bragg peak at ~26.77°. The low-intensity peak is found in the composite sample due to the extremely high-intensity peaks of the $NiSb_2O_6$ sample.

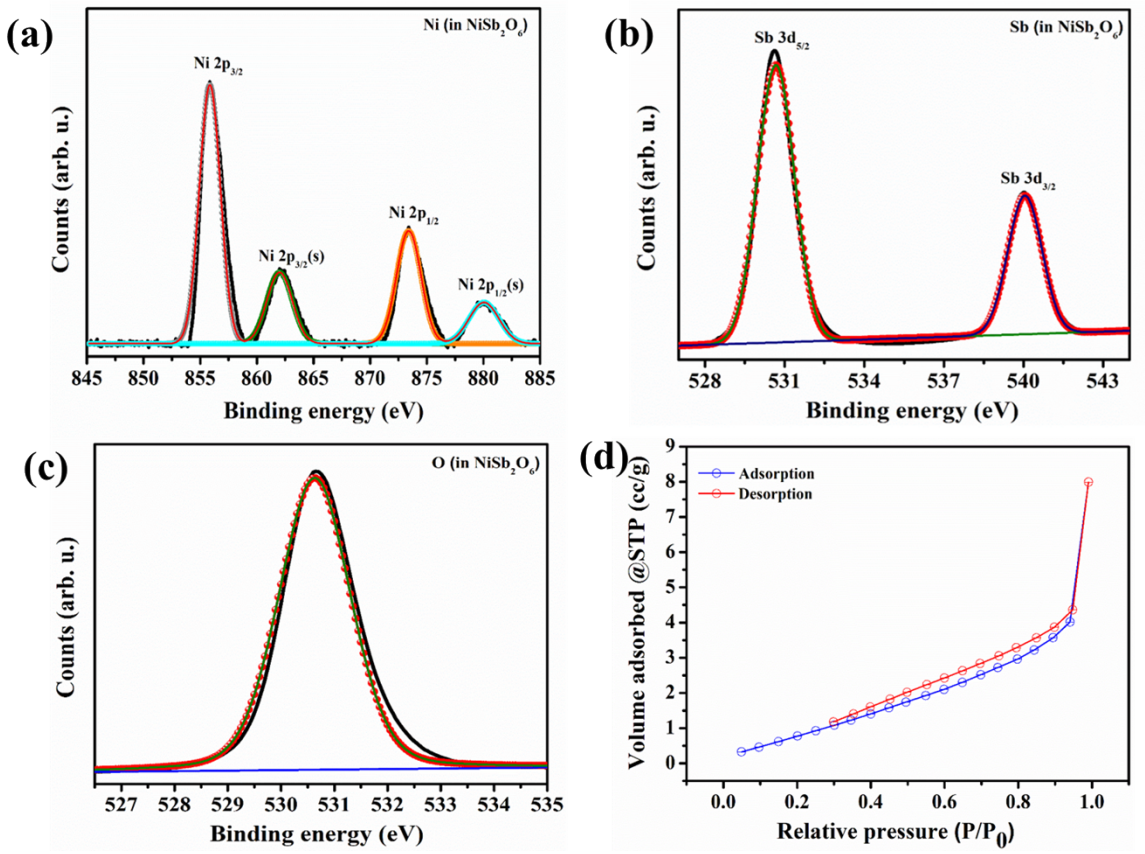

Figure S2 XPS high-resolution spectra for (a) Ni 2p, (b) Sb 3d, (c) O 1s in case of bare $NiSb_2O_6$, (d) BET isotherm of bare $NiSb_2O_6$.

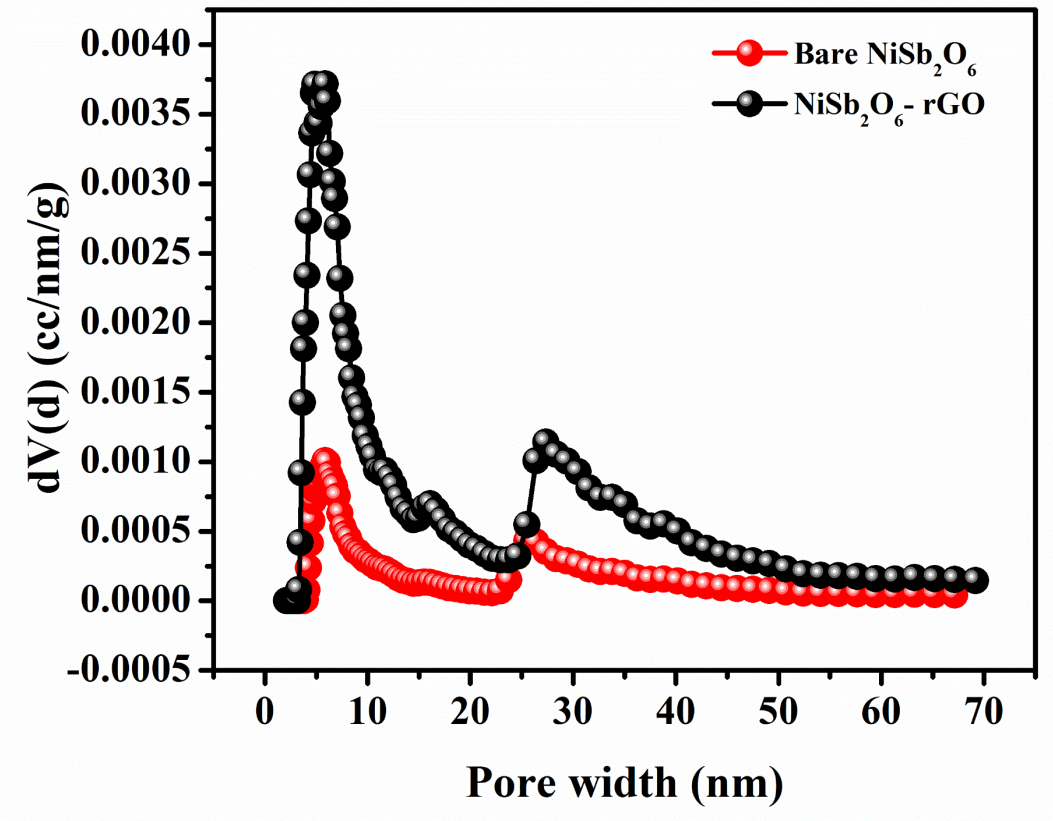

Figure S3 Pore size distribution curve for bare $NiSb_2O_6$ and $NiSb_2O_6$-reduced graphene oxide composite.

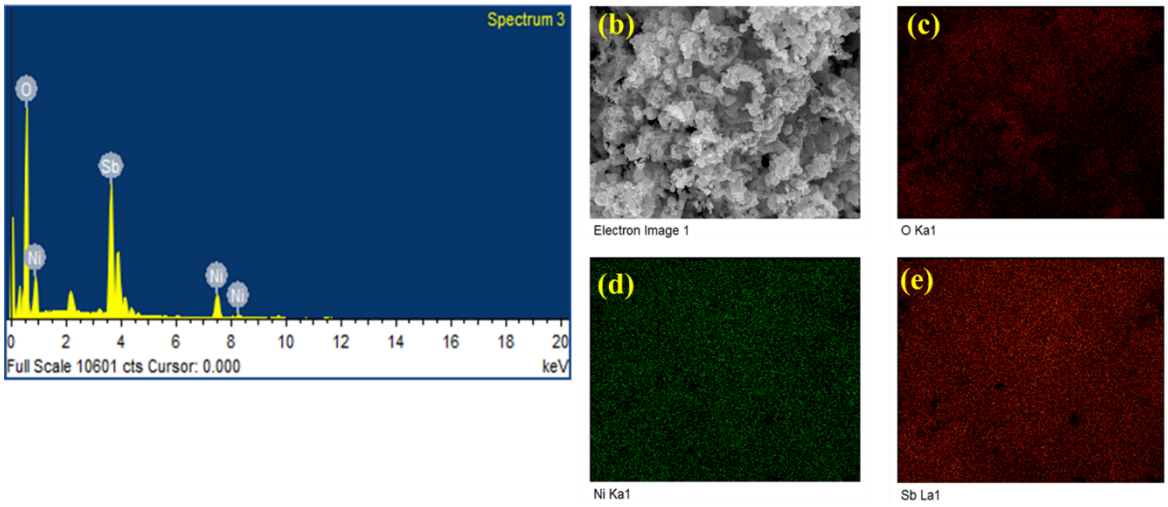

Figure S4 (a) The EDS spectrum $NiSb_2O_6$, (b) FE-SEM micrograph for elemental mapping of $NiSb_2O_6$, (c) oxygen, (d) nickel, (e) antimony.

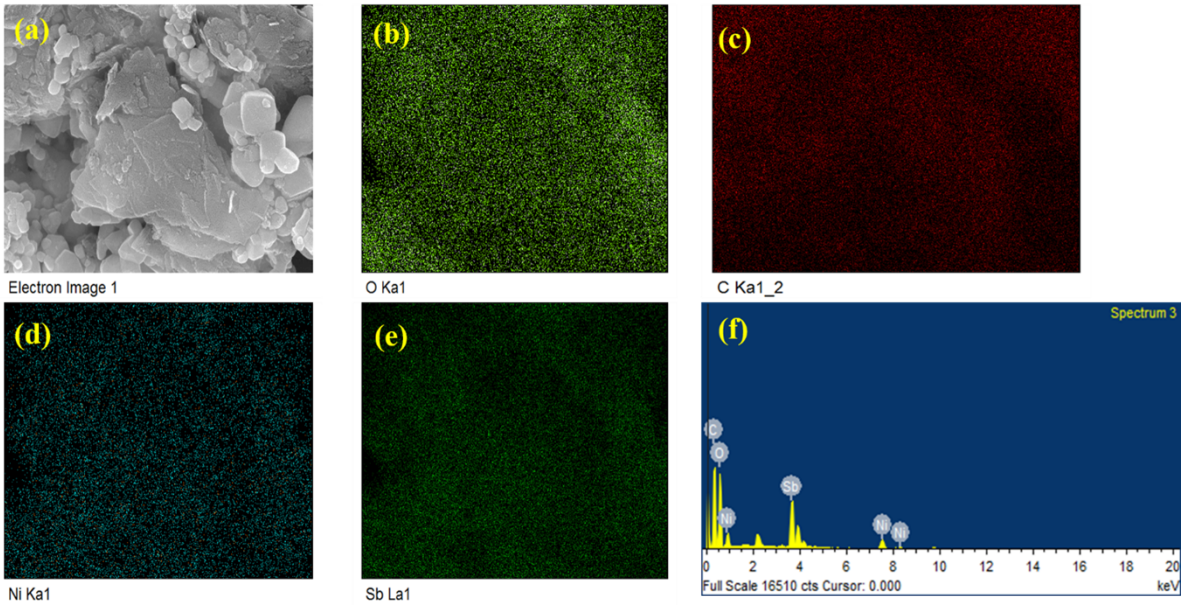

Figure S5 (a) FE-SEM micrograph for elemental mapping of $NiSb_2O_6$, (b) oxygen, (c) carbon, (d) nickel, and (e) antimony, (f) The EDX spectrum $NiSb_2O_6$-reduced graphene oxide composite.

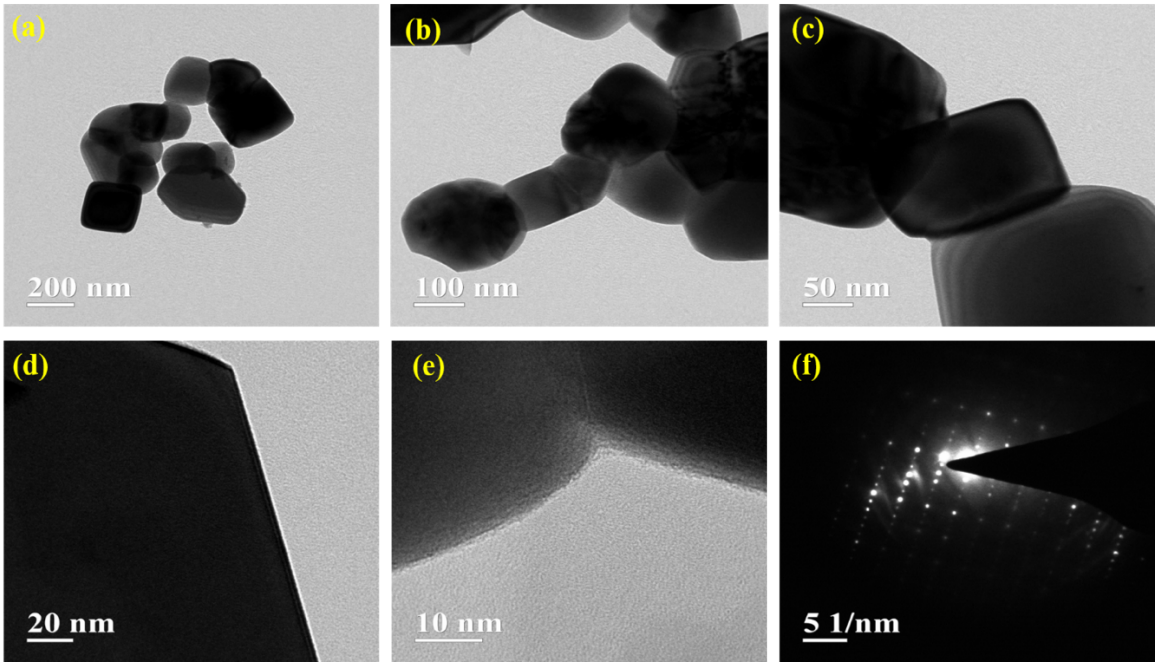

Figure S6 HR-TEM micrographs of $NiSb_2O_6$ different magnifications (a) 200 nm, (b) 100 nm, (c) 50 nm, (d) 20 nm (e)10 nm (d) SAED pattern of $NiSb_2O_6$

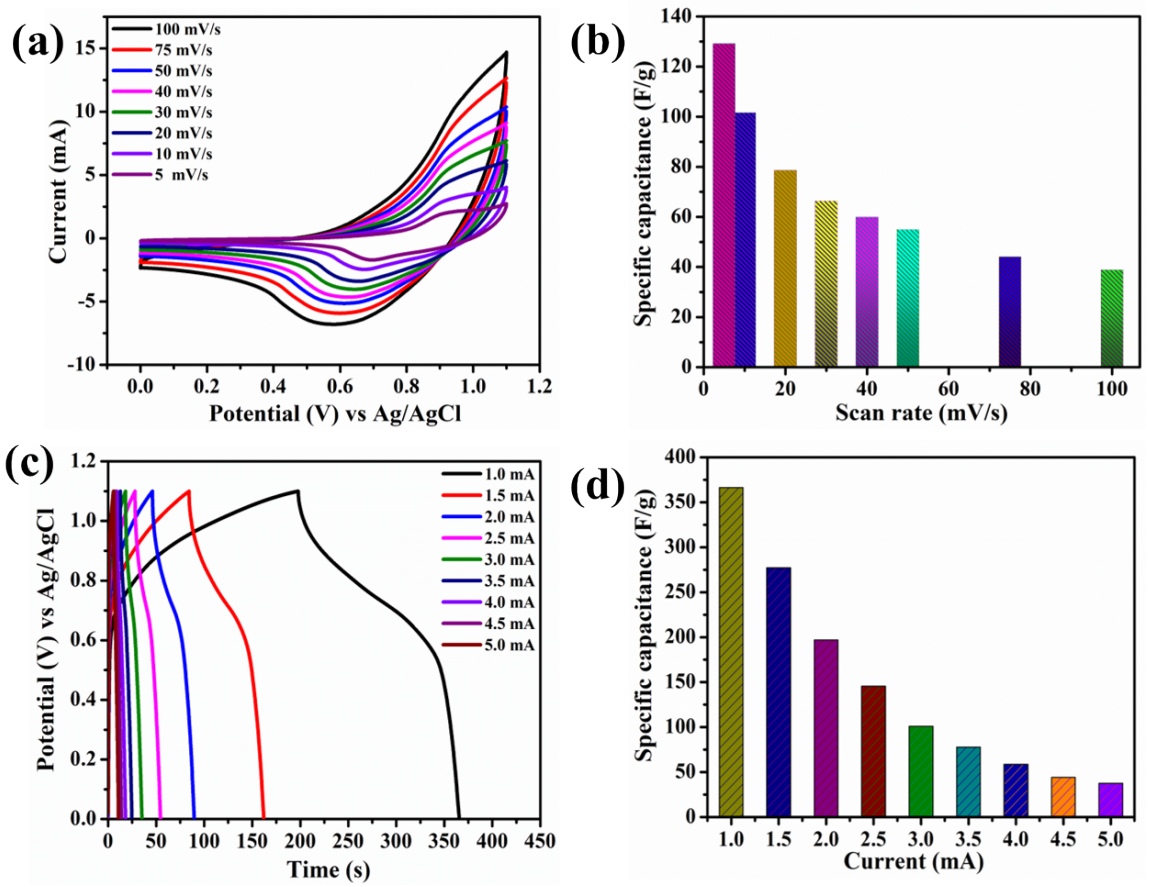

Figure S7 Electrochemical analysis of $NiSb_2O_6$ electrode. (a) CV plots of $NiSb_2O_6$ electrode at various scan rates 5 – 100 mV s^{-1}, (b) effect of scan rates on specific capacitances of $NiSb_2O_6$ electrode, (c) CD plots of $NiSb_2O_6$ electrode at various applied currents and (d) effect of various current values on specific capacitances of $NiSb_2O_6$ electrode.

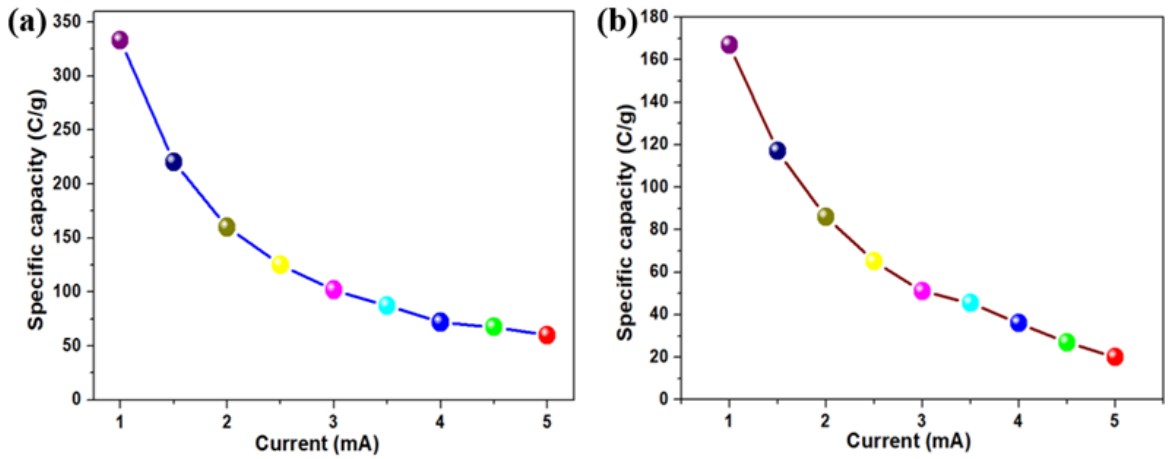

Figure S8 The specific capacity vs. applied current plot for (a) $NiSb_2O_6$-rGO composite electrode and (b) bare $NiSb_2O_6$ electrode.

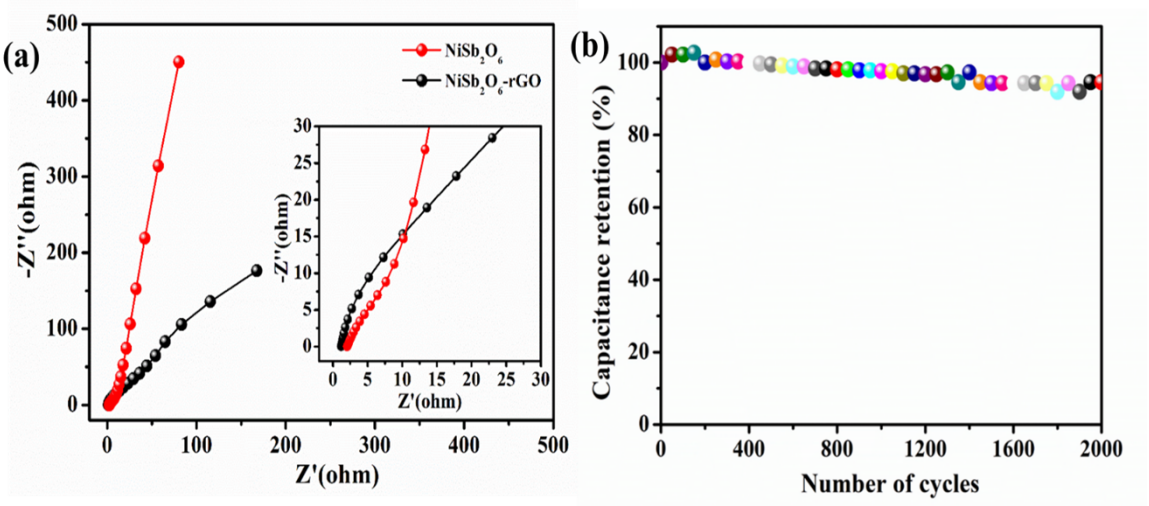

Figure S9 (a) Nyquist plots comparison for $NiSb_2O_6$ and $NiSb_2O_6$–reduced graphene oxide composite electrode, with inset shows the enlarged portion of Nyquist plots $NiSb_2O_6$ and $NiSb_2O_6$–reduced graphene oxide composite electrode, (b) cyclic stability of $NiSb_2O_6$–reduced graphene oxide composite electrode over 2000 cycles.

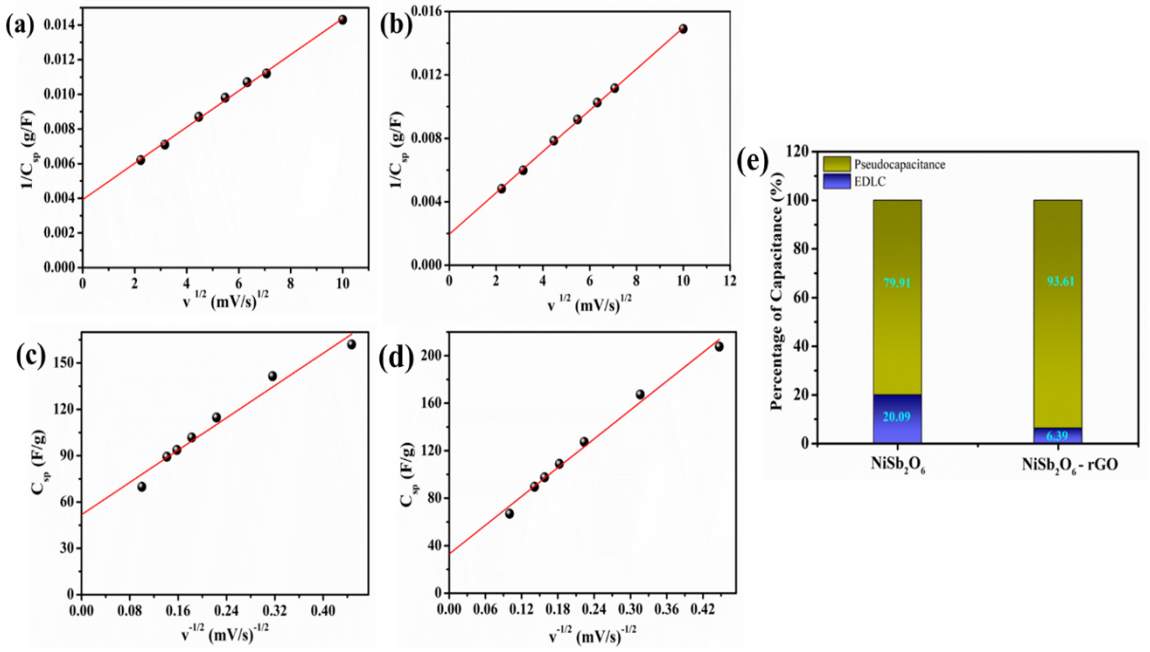

Figure S10 Trasatti plots $NiSb_2O_6$ and $NiSb_2O_6$–reduced graphene oxide composite electrode. The relationship between 1 / C_{sp} and $v_{1/2}$ is examined for two types of electrodes: (a) bare $NiSb_2O_6$ electrode and (b) $NiSb_2O_6$–reduced graphene oxide composite electrode. The relationship between C_{sp} and $v^{-1/2}$ is examined for two different electrodes: (c) bare $NiSb_2O_6$ electrode and (d) $NiSb_2O_6$–reduced graphene oxide composite electrode. These electrodes are tested in Na_2SO_4 electrolyte. (e) The study investigates the contribution of EDLC and pseudocapacitance in the $NiSb_2O_6$ electrode and the $NiSb_2O_6$-reduced graphene oxide composite electrode.

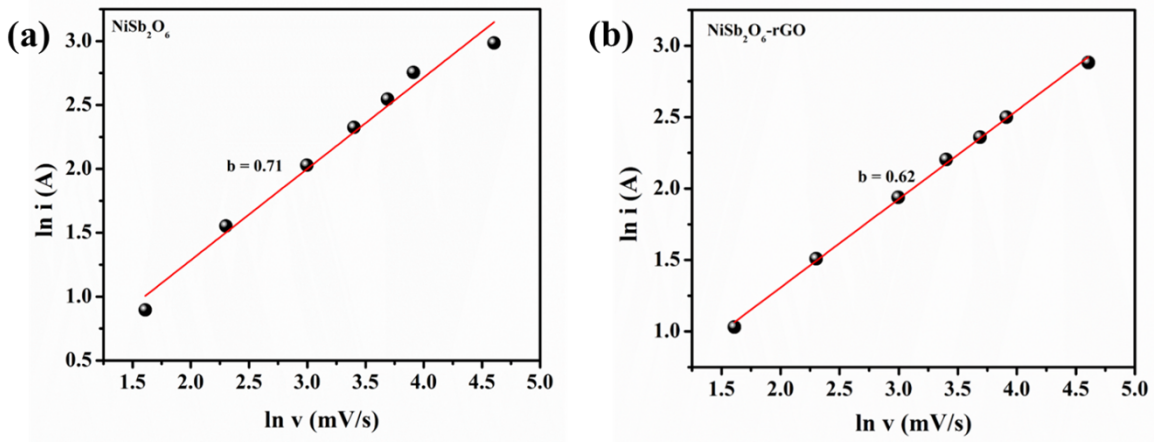

Figure S11 Differentiating the device's nature can be determined by calculating the b parameter using the power law equation. This parameter represents the slope of the linear relationship between the ln of the current and the ln of the scan rate for (a) $NiSb_2O_6$ and (b) $NiSb_2O_6$–reduced graphene oxide composite electrode.

Three-electrode measurement results for $NiSb_2O_6$-rGO composite electrodes with 90:10 and 85:15 ratios;

Figure S12(a) shows the cyclic voltammetry curve for the $NiSb_2O_6$-rGO (90:10) at the different scan rates varying from 5 mV/s to 100 mV/s. **Figure S12(b)** represents the plot for the effect of specific capacitance on scan rates. The maximum specific capacitance of about 357.64 F/g is obtained at a scan rate of 5 mV/s. **Figure S12(c)** shows the charge-discharge profile for the $NiSb_2O_6$-rGO (90:10) at different applied current values (from 1 mA to 5 mA). A maximum specific capacitance of about 1088.6 F/g at the current density of 1 A/g is obtained for the $NiSb_2O_6$-rGO (90:10) electrode as shown in **Figure S12(d).**

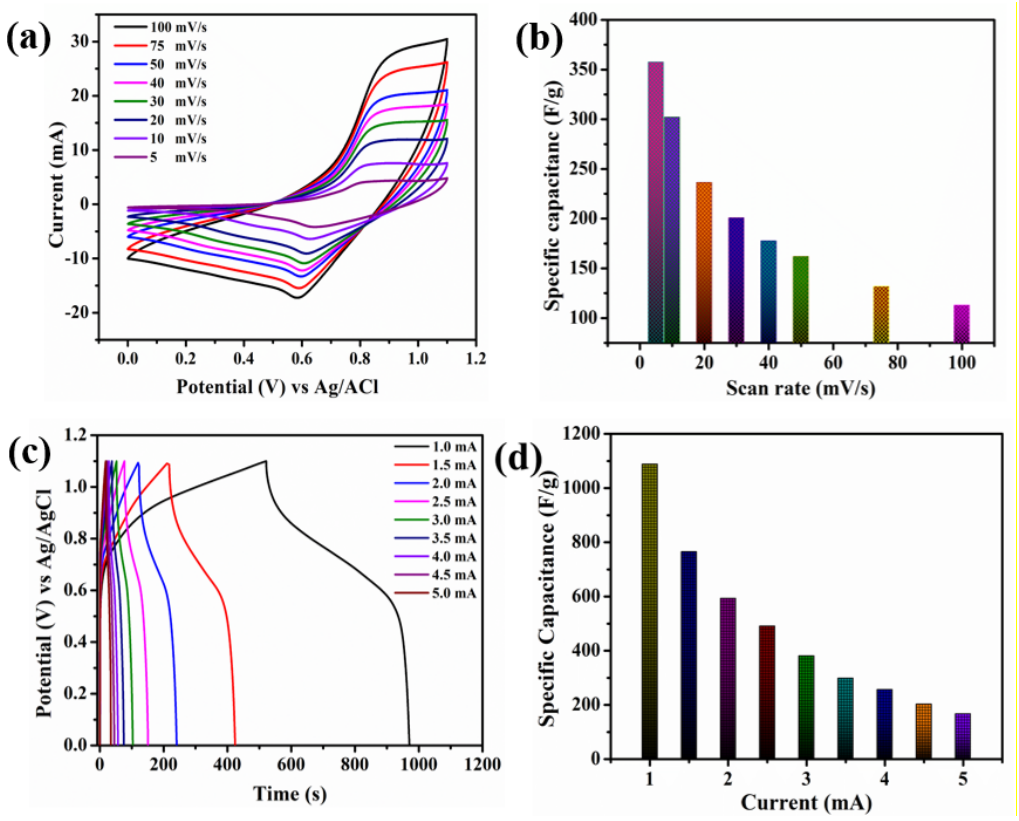

Figure S12 Electrochemical analysis of prepared $NiSb_2O_6$-rGO (90:10) composite (a) cyclic voltammetric curve for different scan rates (from 100 mV/s to 5 mV/s), (b) specific capacitance vs. scan rate curve calculated from CV profile, (c) charge-discharge curve at different applied currents (from 1 mA to 5 mA), and (d) specific capacitance vs. applied current curve calculated from CD profile.

Figure S13(a) shows the cyclic voltammetry curve for the $NiSb_2O_6$-rGO (85:15) at the different scan rates varying from 5 mV/s to 100 mV/s. **Figure S13(b)** represents the plot for the effect of specific capacitance on scan rates. The maximum specific capacitance of around 95 F/g is obtained at a scan rate of 5 mV/s. **Figure S13(c)** shows the charge-discharge profile for the $NiSb_2O_6$-rGO (85:15) at different applied current values (from 1 mA to 5 mA). A maximum specific capacitance of around 250 F/g at the current density of 1 A/g is obtained for the $NiSb_2O_6$-rGO (85:15) electrode as shown in **Figure S13(d).**

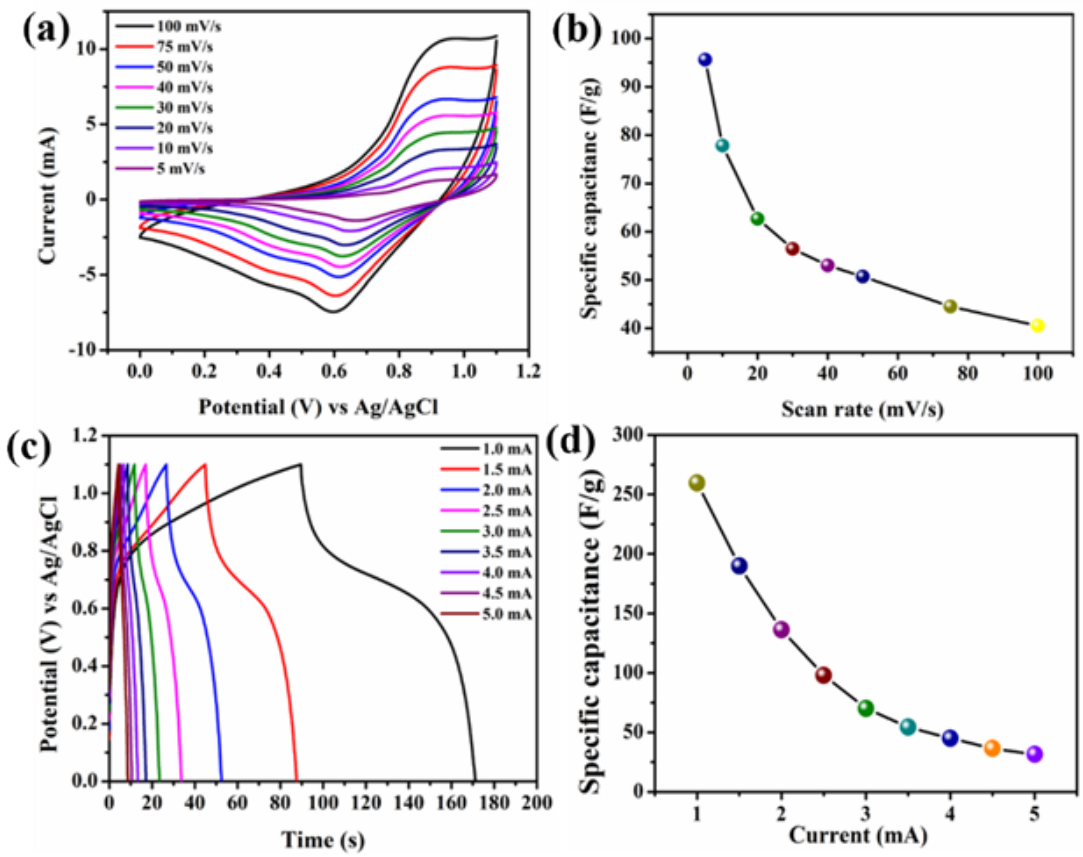

Figure S13. Electrochemical analysis of prepared $NiSb_2O_6$-rGO (85:15) composite (a) cyclic voltammetric curve for different scan rates (from 100 mV/s to 5 mV/s), (b) specific capacitance vs. scan rate curve calculated from CV profile, (c) charge-discharge curve at different applied currents (from 1 mA to 5 mA), and (d) specific capacitance vs. applied current curve calculated from CD profile.

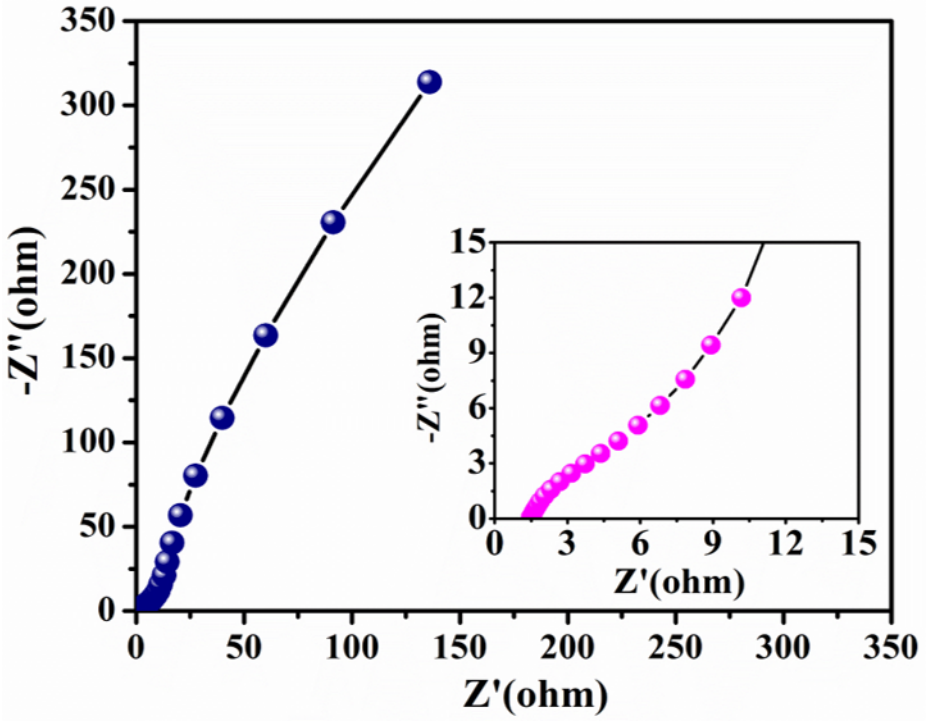

Figure S14 Nyquist plot, showing the impedance characteristic of the $NiSb_2O_6$–reduced graphene oxide composite symmetric cell device, with an expanded view shown in the inset.

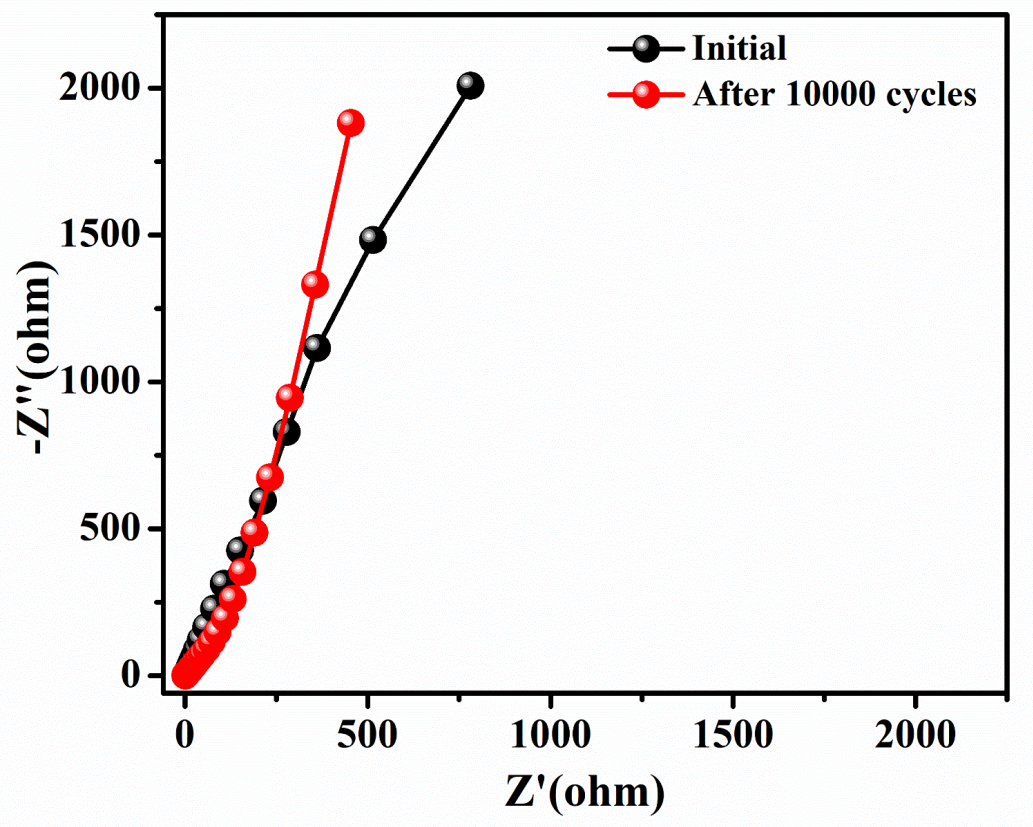

Figure S15 Nyquist plots comparison for $NiSb_2O_6$–reduced graphene oxide composite symmetric cell device, taken during the initial phase and following the cyclic stability test.

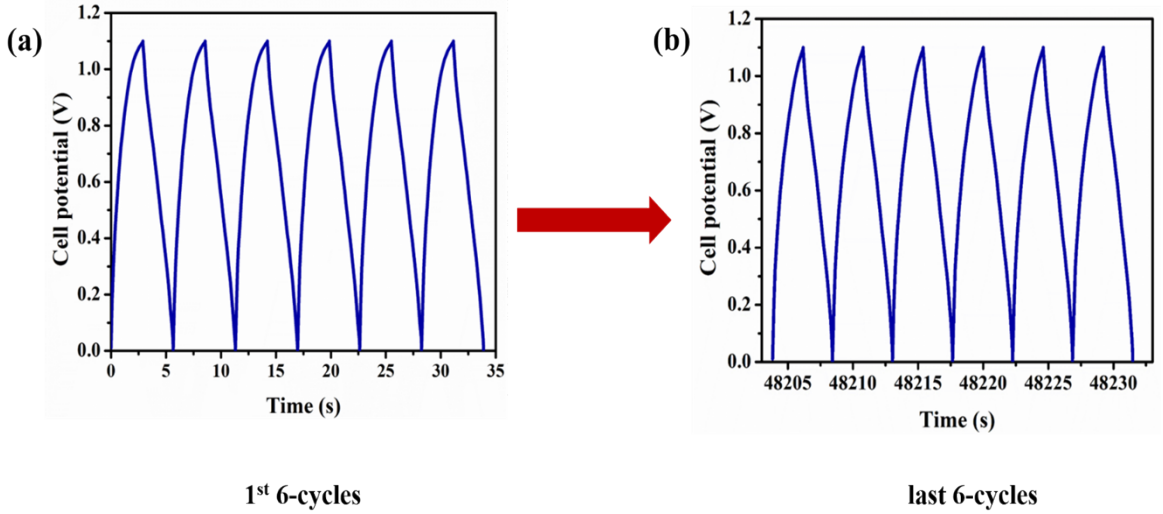

Figure S16 The first six and final six cycles of $NiSb_2O_6$–reduced graphene oxide composite symmetric cell device, obtained from the cyclic stability test.

Table S1: Review of the supercapacitive performances of the $NiSb_2O_6$–reduced graphene oxide composite electrode and other released research for supercapacitor electrodes, as evaluated utilizing the three-electrode system.

Sr no.	Material name	Preparation Methods	Specific capacitance (F/g)	References
1.	RuSbO-G	Microwave-assisted method	236	[1]
2.	Cu_3SbS_4	Facial one-pot hydrothermal	41.785	[2]
3.	Fe_3O_4-graphene	Hydrothermal	81	[3]
4.	ZnO-graphene	Sol-gel	95	[4]
5.	ZnO-graphene	Microwave technique	109	[5]
6.	CuO	Wet Chemical method	88.5	[6]
7.	$FeMoS_2$-graphene	Hydrothermal	135	[7]
8.	$ZnSb_2O_6$	Precipitation method	140.8	[8]
9.	RGOSb	Modifies Staudenmaier method	289	[9]
10.	NiO-rGO	Hydrothermal	171.3	[10]
11.	NiO	Hydrothermal	137.7	[11]
12.	Sb-SnO2	Facile co-precipitation	158.2	[12]
13.	**$NiSb_2O_6$-rGO**	**Solid-State**	**952.38**	**This Work**

Reference:

[1] P. Ekwere *et al.*, "High stability asymmetric supercapacitor cell developed with novel microwave-synthesized graphene-stabilized ruthenium antimonide nanomaterial," *J. Energy Storage*, vol. 63, no. February, p. 106853, 2023, doi: 10.1016/j.est.2023.106853.

[2] V. K. Mariappan, K. Krishnamoorthy, P. Pazhamalai, S. Sahoo, and S. J. Kim, "Layered famatinite nanoplates as an advanced pseudocapacitive electrode material for supercapacitor applications," *Electrochim. Acta*, vol. 275, pp. 110–118, 2018, doi: 10.1016/j.electacta.2018.04.126.

[3] Z. Song, W. Liu, P. Xiao, Z. Zhao, G. Liu, and J. Qiu, "Nano-iron oxide (Fe2O3)/three-dimensional graphene aerogel composite as supercapacitor electrode materials with extremely wide working potential window," *Mater. Lett.*, vol. 145, pp. 44–47, 2015, doi: 10.1016/j.matlet.2015.01.040.

[4] I. Y. Y. Bu and R. Huang, "One-pot synthesis of ZnO/reduced graphene oxide nanocomposite for supercapacitor applications," *Mater. Sci. Semicond. Process.*, vol. 31, pp. 131–138, 2015, doi: 10.1016/j.mssp.2014.11.037.

[5] A. Ramadoss and S. J. Kim, "Facile preparation and electrochemical characterization of graphene/ZnO nanocomposite for supercapacitor applications," *Mater. Chem. Phys.*, vol. 140, no. 1, pp. 405–411, 2013, doi: 10.1016/j.matchemphys.2013.03.057.

[6] Y. X. Zhang, M. Huang, F. Li, and Z. Q. Wen, "Controlled synthesis of hierarchical CuO nanostructures for electrochemical capacitor electrodes," *Int. J. Electrochem. Sci.*, vol. 8, no. 6, pp. 8645–8661, 2013, doi: 10.1016/s1452-3981(23)12916-6.

[7] Y. Wang, P. He, W. Lei, F. Dong, and T. Zhang, "Novel FeMoO4/graphene composites based electrode materials for supercapacitors," *Compos. Sci. Technol.*, vol. 103, pp. 16–21, 2014, doi: 10.1016/j.compscitech.2014.08.009.

[8] M. Balasubramaniam and S. Balakumar, “Exploration of electrochemical properties of zinc antimonate nanoparticles as supercapacitor electrode material,” *Mater. Sci. Semicond. Process.*, vol. 56, no. August, pp. 287–294, 2016, doi: 10.1016/j.mssp.2016.09.014.

[9] M. Ciszewski, A. Mianowski, G. Nawrat, and P. Szatkowski, “Reduced Graphene Oxide Supported Antimony Species for High-Performance Supercapacitor Electrodes,” *ISRN Electrochem.*, vol. 2014, pp. 1–7, 2014, doi: 10.1155/2014/826832.

[10] J. Xu *et al.*, “NiO-rGO composite for supercapacitor electrode,” *Surfaces and Interfaces*, vol. 18, no. December 2019, 2020, doi: 10.1016/j.surfin.2019.100420.

[11] Y. zhen Zheng, H. yang Ding, and M. lin Zhang, “Preparation and electrochemical properties of nickel oxide as a supercapacitor electrode material,” *Mater. Res. Bull.*, vol. 44, no. 2, pp. 403–407, 2009, doi: 10.1016/j.materresbull.2008.05.002.

[12] J. Zhang, Y. Sun, and J. Xu, “Fabrication of antimony doped tin oxide nanopowders as an advanced electrode material for supercapacitors,” *Micro Nano Lett.*, vol. 14, no. 3, pp. 254–258, 2019, doi: 10.1049/mnl.2018.5212.